Case Studies in Fire Safety 4 (2015) 11–18

Contents lists available at ScienceDirect

Case Studies in Fire Safety

journal homepage: www.elsevier.com/locate/csfs

Short communication

Modeling wildland fire propagation using a semi-physical network model

J.K. Adou [a], A.D.V. Brou [b,*], B. Porterie [c]

[a] Université FHB de Cocody, UFR Math. Info., 22 BP 582 Abidjan 22, Cote d'Ivoire
[b] Université JLoG de Daloa, UFR Environnement, BP 150 Daloa, Cote d'Ivoire
[c] Aix Marseille Université, CNRS, IUSTI UMR 7343, 13453 Marseille, France

ARTICLE INFO

Article history:
Received 16 October 2014
Received in revised form 23 April 2015
Accepted 10 May 2015
Available online 28 June 2015

Keywords:
Wildland fire
Rate of spread
Heat transfer
Network model
Sensitivity analysis

ABSTRACT

In this paper we present a surface wildfire model which can be used to develop and test new firefighting strategies and land use planning practices. This model is simple, easy to implement and can predict the rate of fire spread, the fire contour and both burning and burned areas. It also incorporates weather conditions and land topography. The predictive capability of the model is partially assessed by comparison with data from laboratory-scale and prescribed burning experiments. A sensitivity analysis is conducted to identify the most influential input model parameters controlling fire propagation.

1. Introduction

With global warming and ever-increasing urban-interface areas, forest fires have become a major issue in terms of human casualties, economic losses, and environmental damage. Fire modeling is used to understand and to predict possible fire behavior. Fire propagation models belong to different types depending on the approach they use. They are divided into stochastic and deterministic models, the latter being either empirical or based on the laws of physics. The model developed by Porterie et al. [1,2] combines the features of a stochastic network model with those of a semi-physical model of the interaction between the fire front and the vegetative fuel. As stated in [3], it has the advantage of taking into account physical effects well beyond the nearest neighbors of a burning site, such as flame-induced radiative effects or firebrand impact. This model combines the solid flame model and the Monte Carlo method to calculate radiation. However, this model does not take into account heat transfer by convection [3], which plays an important role in wind-driven surface fires. Indeed, as shown in [4,5], on a wide range of scales for relatively low fuel loads, fire spread is mainly governed by convective heat transfer. To take into account this important mechanism of heat transfer, the above-mentioned radiation-driven fire model is coupled with the thermal model of Koo et al. [6], in which vegetation is considered as a porous fuel layer through which the fire spreads by convection and radiation.

This paper is organized as follows. First, the one-dimensional thermal model is extended to two dimensions where vegetation is depicted as a regular network of combustible cells. Second, we compare model results with data from

* Corresponding author.
E-mail address: brou_david2003@yahoo.fr (A.D.V. Brou).

http://dx.doi.org/10.1016/j.csfs.2015.05.003

laboratory-scale and prescribed burning experiments. Third, a sensitivity analysis is conducted to identify the most influential input model parameters controlling fire propagation. Finally, in the last section conclusions are drawn and recommendations are made for future work.

2. The model

The present model is built from a two-dimensional regular network of equal-size square cells, with a density p of combustible cells (*i.e.* a cell which contains forest fuel), the $1-p$ remaining cells being either empty or filled with non-combustible elements (Fig. 1). Combustible cells can be distributed either randomly (for statistical purposes) or deterministically using a vegetation map of the study area. It is assumed that each combustible cell j has a cylindrical shape with a height H_j and a diameter D_j. A combustible cell j is said to be healthy when its temperature T_j is equal to the ambient temperature T_∞. The energy absorbed by the combustible cell when it is exposed to the fire front is used to raise the temperature of wet fine fuel elements to the boiling temperature of water, 373 K, evaporate the moisture, and raise the temperature of dry fine fuel elements to the ignition temperature. The combustible cell then continues to burn with a flame for a duration t_c (flame residence time), while transferring heat to the neighboring cells by means of convection and radiation. In the solid flame model, the visible flame is regarded as a uniformly radiating solid body with a cylindrical shape and with thermal radiation emitted from its surface.

The temperature of a cell is determined using the equation of energy conservation [6,7].

Let us consider a combustible cell j located at a distance d_{ij} from the burning cell i (Fig. 1). The total heat flux q_{ij} emitted from the burning cell i which is received by cell j is given by [6]:

$$q_{ij} = \underbrace{q_{ij}^{sr}}_{\substack{\text{surface}\\ \text{radiation}}} + \underbrace{q_{ij}^{ir}}_{\substack{\text{internal}\\ \text{radiation}}} + \underbrace{q_{ij}^{sc}}_{\substack{\text{surface}\\ \text{convection}}} + \underbrace{q_{ij}^{ic}}_{\substack{\text{internal}\\ \text{convection}}} + \underbrace{q_{ij}^{rl}}_{\substack{\text{radiative}\\ \text{loss}}} \tag{1}$$

The right-hand side of Eq. (1) is the sum of all possible heat transfer mechanisms: radiation on the top surface of cell j, internal radiation from the ember zone, convection on the top surface of cell j, internal convection inside the fuel bed, and radiation loss to the ambient at the top surface of cell j. For most nonzero ambient flow velocities, as is the case in the present study, the other energy-transfer mechanisms of preheating, such as turbulent diffusion, solid- and gas-phase conduction, convective cooling, as well as the energy absorbed by pyrolysis prior to ignition, may be disregarded [7]. Each term in Eq. (1) is examined below.

Only fine thermally thin vegetative fuels (*e.g.*, grass and foliage of shrubs and trees) are considered since they are responsible for the spread of fire, with thicker fuel elements burning more slowly at the back of the fire front. Fine fuels are defined as organic material less than 6 mm in diameter [8].

The energy q_{ij} absorbed by cell j is used on the one hand to raise the temperature of fine fuel elements and on the other hand to evaporate moisture at the boiling temperature of water,

$$q_{ij} = \begin{cases} \rho_j C_{pj} \phi_j \dfrac{dT_j}{dt}, & \text{for } T_j \neq 373\ \text{K} \\ -\rho_j h_{vap} \phi_j \dfrac{dW_j}{dt}, & \text{for } T_j = 373\ \text{K} \end{cases} \tag{2}$$

where T_j and W_j are respectively the mean temperature and the mass fraction of water of cell j, *i.e.* the mass of water per unit of initial wet fuel bed mass. In Eq. (2) ρ_j is the fuel particle density, C_{pj} is the specific heat capacity, h_{vap} is the specific enthalpy change of water to vapor at 373 K, and ϕ_j is the packing ratio, *i.e.* the fraction of the fuel bed volume filled with fine fuel elements. Their packing ratio may be deduced from the formula $\phi_j = M_j/H_j\rho_j$ where M_j is the initial mass of fine fuels per unit area and H_j the height of the vegetative cell j.

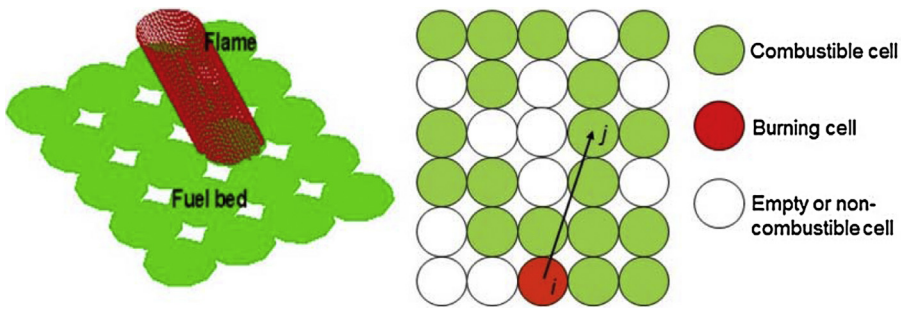

Fig. 1. Solid flame model (left) and schematic of the network showing the interaction between a burning cell i and a healthy cell j (right).

Radiation from the flame to cell j on the top surface of the fuel bed is:

$$q_{ij}^{sr} = \frac{a_{fb}\varepsilon_{fl}\sigma T_{fl}^4}{H_j} F_{ij} \tag{3}$$

where $\varepsilon_{fl} = 1 - \exp(-0.6L_{fl})$ is the flame emissivity [6,9], a_{fb} is the fuel bed absorptivity, and σ (=5.67 × 10^{-8} W/m^2/K) is the Stephan–Boltzmann constant. The visible flame is regarded as a uniformly radiating surface with a cylindrical geometry (Fig. 1). The view factor F_{ij} is the fraction of the radiation from the burning cell i which is intercepted by cell j. It is determined by an area integral method [10]. The emitting flame surface is divided into small parallelograms (Fig. 1). The view factor between a parallelogram element A_p and the infinitesimal area of cell j is thus given by:

$$F_{ij} = \sum_{\substack{\text{all elements} \\ \text{where } \cos\theta_1 > 0 \\ \text{and } \cos\theta_2 > 0}} \frac{\cos\theta_1 \cos\theta_2 A_P}{\pi r^2} \tag{4}$$

where r is the distance between the center O_1 of the small parallelogram element and cell j, $r = \|\vec{O_1 j}\|$, θ_1 is the angle between the vector $O_1 j$ and the outward normal to the parallelogram element, and θ_2 is the angle between jO_1 and the normal to cell j.

Within the porous fuel bed, the unburned cell receives radiative heat flux through the fuel bed volume from the burning embers at the flame front. This internal radiation to cell j at the distance d_{ij} is [6]:

$$q_{ij}^{ir} = 0.25A_{fb}\varepsilon_b\sigma T_b^4 \exp(-0.25A_{fb}d_{ij}) \tag{5}$$

Following Koo et al. [6], the ember emissivity ε_b is assumed to be one and the ember temperature T_b to be the ignition temperature. A_{fb} is the total fuel-particle surface area per fuel-bed volume.

The unburned cell loses heat to the ambient by radiation at the top surface of the fuel bed:

$$q_{ij}^{rl} = -\frac{\varepsilon_{fb}\sigma(T_j^4 - T_\infty^4)}{H_j} \tag{6}$$

where ε_{fb} is the fuel bed emissivity.

Only forced convective heat transfer due to the ambient wind is considered. The convective heat transfer to the top surface of cell j is:

$$q_{ij}^{sc} = \frac{0.565k_{fl}Re_{d_{ij}}^{1/2}Pr^{1/2}}{d_{ij}H_j}(T_{fl} - T_j)\exp(-0.3d_{ij}/L_{fl})\beta_{ij} \tag{7}$$

Pr is the Prandtl number and the Reynolds number based on the length scale d_{ij} and the ambient wind U_w, $Re_{d_{ij}} = U_w d_{ij}/\nu_g$. The thermal conductivity k_{fl} and the kinematic viscosity ν_g are assumed to be those of air at the flame temperature.

The convective heat transfer coefficient for a single cylinder in a cross flow is used for the interior of the fuel bed [6,11]:

$$q_{ij}^{ic} = \frac{0.911A_{fb}k_b Re_D^{0.385}Pr^{1/3}}{D_j}(T_b - T_j)\exp(-0.25A_{fb}d_{ij})\beta_{ij} \tag{8}$$

where $Re_{D_j} = U_{fb}D_j/\nu_g$ is the Reynolds number based on the length scale D_j and the velocity of wind inside the fuel bed, $U_{fb} = (1-\phi_j)U_w \cdot \beta_{ij}$ is a coefficient which is equal to unity when the straight line connecting cells i and j is aligned with the wind direction, and zero otherwise.

Finally, prior to ignition ($0 \le t \le t_c$), the system of ordinary differential equations to be solved may be written as

$$\begin{cases} \dfrac{dT_j}{dt} = \dfrac{1}{\rho_j C_{pj}\phi_j}\displaystyle\sum_{l=sr,ir,sc,ic,rl} q_{ij}^l, & \text{for } T_j \neq 373\text{ K} \\ \dfrac{dW_j}{dt} = -\dfrac{1}{\rho_j h_{vap}\phi_j}\displaystyle\sum_{l=sr,ir,sc,ic,rl} q_{ij}^l, & \text{for } T_j = 373\text{ K} \end{cases} \tag{9}$$

with the initial conditions: $T_j(0) = T_\infty$, $W_j(0) = W_0$, where W_0 is the initial mass fraction of water. Eq. (9) is solved numerically using a fourth-order Runge–Kutta method to determine the temperature and water mass of cell j. One of the features of the present model is that, given the mechanisms of preheating considered, each burning cell has its own interaction domain. Therefore we only follow the thermal response of the receptive cells located in the interaction domains of the burning cells, which significantly reduces CPU time and memory allocation.

Table 1
Model input data.

Experiment	Weise (white birch)	C064	F19
Flame length (m)	0.08–1.69	4.0	5.0
Ambient wind speed (m/s)	0–1.15	4.6	4.8
Fuel bed slope (°)	−15 to +15	0	0
Initial water mass fraction (–)	0.11	0.063	0.058
Fuel bed thickness (m)	0.114	0.21	0.51
Ambient temperature (K)	303	305	307
Flame temperature (K)	1083	1083	1083
Ignition temperature (K)	500	500	500
Fuel density (kg/m^3)	609	512	512
Surface-to-volume ratio of fuel particles (m^{-1})	17.5	25.4	14.6
Fuel bed absorptivity (–)	0.6	0.6	0.6
Fuel bed emissivity (–)	0.9	0.6	0.6
Density p of combustible cells (%)	80	100	100

3. Results

The fire spread model was applied to two different fire scenarios: laboratory-scale experiments on white birch in a wind tunnel [12] and grassland fire experiments conducted in the Northern Territory of Australia, referred to as C064 and F19 [13]. The main parameters used for the simulations are summarized in Table 1. The flame residence time t_c is taken as being greater than the ignition time.

3.1. Laboratory-scale experimental data

Weise's experimental data for flame spread on very porous white birch fuel beds in a laboratory wind tunnel are compared with model results. A tilted wind tunnel was employed with an adjustable roof and a test section 2.52 m long by 0.69 m wide. Wind and fire directions coincide. The rate of spread and the flame length are recorded for different wind speeds and slopes. For more details see [12,14].

The data used are the same as those used in [6]. The size of each cell is taken as being equal to 0.1 m and the time step is 1 s (Fig. 2).

Fig. 3 compares model results and measurements for the rate of spread. One can observe that the model slightly overestimates spread rates, especially when the fire propagates slowly. The relative error between predicted and experimental flame spread rates $ERR = \frac{\|y_{\exp}(x) - y_{th}(x)\|_{L^2}}{\|y_{\exp}(x)\|_{L^2}}$ is approximately 7%, showing a good overall agreement.

3.2. Large-scale experimental burns

We also compare model results with data reported by Cheney et al., who conducted grassland experiments in the Northern Territory of Australia during July and August 1986 [13,15,16]. Fuels were open grasslands, and grasses were continuous and fully cured. Here we focus on two experiments. In the first experiment, referred to as *C064*, the fuel is *Eriachne* grass with a mean surface-area-to-volume ratio of 9770 m^{-1} and a mean fuel load equal to 0.283 kg/m^2. The size of the grassland plot is 104 m × 108 m. The fire was lit from a 50 m-long ignition line perpendicular to the prevailing wind on the upwind edge of the plot. The ignition line fire was created with drip torches carried by two field workers walking for 26 s in opposite directions from the center point to the ends of the line fire. The diameter of each cell is taken as being equal to 1 m. In the second experiment, called *F19*, the fuel is *Themeda* grass with a mean surface-area-to-volume ratio of 12,240 m^{-1}

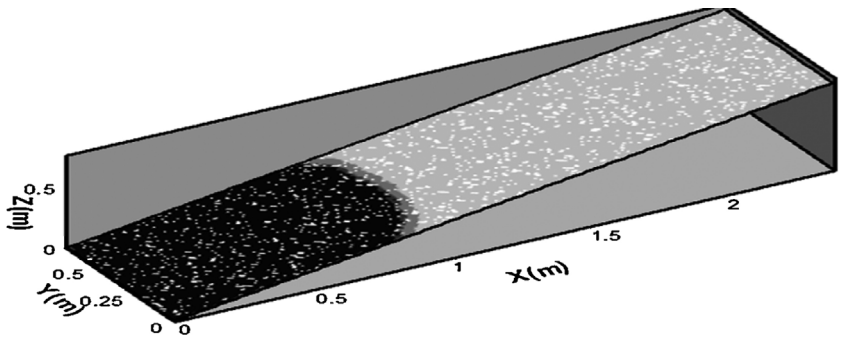

Fig. 2. Weise's experiment [12]: here the slope is 30°. Black cells are burned, gray cells are healthy and at the interface there are burning cells. White cells are non-combustible.

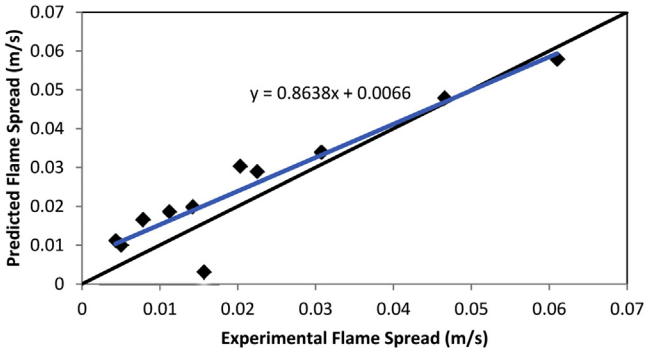

Fig. 3. Comparison of predicted and measured flame spreads for white birch fuel in a wind tunnel for various wind and slope conditions. The blue line represents the best linear fit. (For interpretation of the references to color in this figure legend, the reader is referred to the web version of this article.)

and a mean fuel load equal to 0.313 kg/m^2. The size of the grassland plots is 200 m $\times$ 200 m and the ignition line fire is 175 m long and created in a duration of 56 s in opposite directions. Here, the size of the cells is equal to 1.6 m. Fuel bed characteristics are given in Table 1 for both experiments. Fuel properties that are not provided by the authors are obtained from the literature. The wind speed at 2 m above ground level at each corner of the experimental plots was measured at 5 s intervals throughout the duration of the fire.

In Figs. 4 and 5, we compare the fire contours predicted by our model with those observed in experiments C064 and F19 [13,15]. For experiment C064, the fire contours predicted by our model at 27 s and 53 s are in relatively good agreement with those measured. However, at 100 s, this agreement deteriorates. This discrepancy can be explained by a change in wind direction during the burning [13,15,17], which renders the subsequent comparison unreliable.

Regarding experiment F19, the fire spread rate is significantly underestimated by the model (Fig. 5). Moreover, this underestimation increases with time. At 138 s, the predicted fire contour is less advanced than the real fire contour with an offset of the axis of propagation. The lack of accurate data on the time evolution of wind direction and speed could also explain these differences.

4. Sensitivity study

The predictive capability of the fire spread model presented above depends on the accuracy with which these parameters are determined. Unfortunately, most of them are difficult to measure and/or exhibit a high degree of variability, which in turn makes the output uncertain. The purpose of this section is to answer the following question: which of the model parameters have the greatest influence on model outputs, and thus should serve as guides to future research in the field. A sensitivity study is conducted, which is based on a full factorial design, involving height input parameters, each at two levels ($j = 1, 2$). These eight parameters (or factors $X_i = 1, \ldots, 8$) are given in Table 2. This factorial design thus requires $2^8 = 256$ model runs. Here, the rate of fire spread is considered as the system response. The range of parameter variations is somewhat arbitrary but it is broad enough to cover typical fuel and meteorological conditions (Table 2).

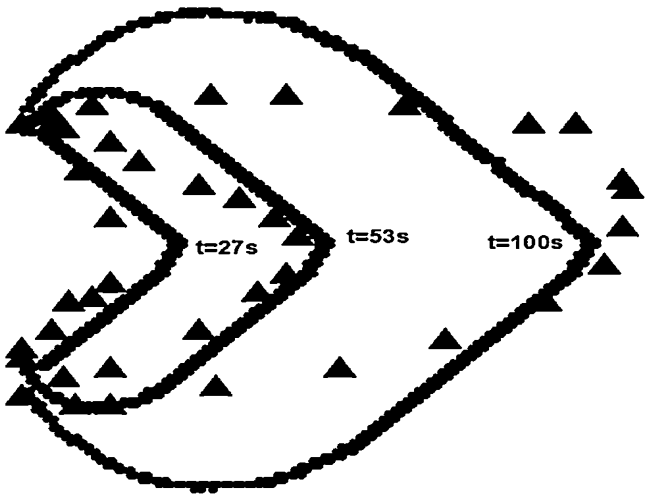

Fig. 4. Australia grassland fire C064 [13,15]: comparison between predicted (bold lines) and real (symbol lines) fire contours.

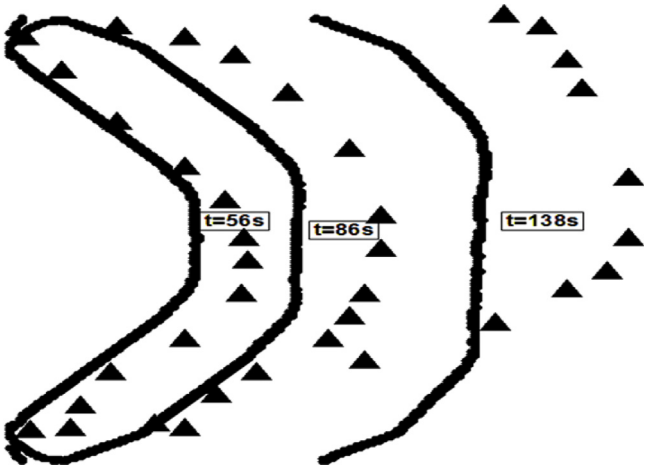

Fig. 5. Australia grassland fire F19 [13,15]: comparison between predicted (bold lines) and real (symbol lines) fire contours.

Table 2
Parameters of the sensitivity analysis and range of variations.

Parameter	Description	Variation	Level 1	Reference value	Level 2
X_1	Flame length (m)	±30	1.183	1.69	2.197
X_2	Ambient wind speed (m/s)	±30	0.805	1.15	1.495
X_3	Initial water mass fraction	±25	0.0825	0.11	0.1375
X_4	Flame temperature (K)	±15	921	1083	1245
X_5	Ignition temperature (K)	±10	450	500	550
X_6	Fuel density (kg/m^3)	±30	426	609	792
X_7	Density of combustible cell (%)	±25	60	80	100
X_8	Fuel specific heat (J/kg K)	±25	1875	2500	3125

Table 3
Effect of parameters on the rate of fire spread.

Parameter	Level	Average	Gap
Flame length	1	0.04228	−0.0035
	2	0.0493	0.0035
Ambient wind speed	1	0.0400	−0.0057
	2	0.0515	0.0057
Initial water mass fraction	1	0.0493	0.0035
	2	0.0422	−0.0035
Flame temperature	1	0.0244	−0.0213
	2	0.0672	0.0213
Ignition temperature	1	0.0581	0.0122
	2	0.0335	−0.0122
Fuel density	1	0.0586	0.0128
	2	0.0329	−0.0128
Density of combustible cell	1	0.0418	−0.0040
	2	0.0498	0.0040
Fuel specific heat	1	0.0530	0.0072
	2	0.0386	−0.0072

M are the modalities tested when the parameters $X_i = 1, \ldots, 8$ are fixed at levels $j = 1,2$. Average y_{ij} system response of the parameter X_i at level j is given by:

$$y_{ij} = \frac{1}{n} \sum_{m \in M} y_m \tag{10}$$

With $n = card(M) = 128$ modalities and y_m is the system response at the modality m. At each level j of parameter X_i, the gap is calculated from: $y_{ij} - Y$, where Y is the rate of spread averaged over the 256 runs. The results are shown in Table 3.

The curves of the effects of the parameters on the rate of fire spread (ROS) are plotted in Fig. 6 and the standard deviations in Fig. 7. In these main-effect figures, nearly horizontal lines indicate little effect. It can be observed that the flame

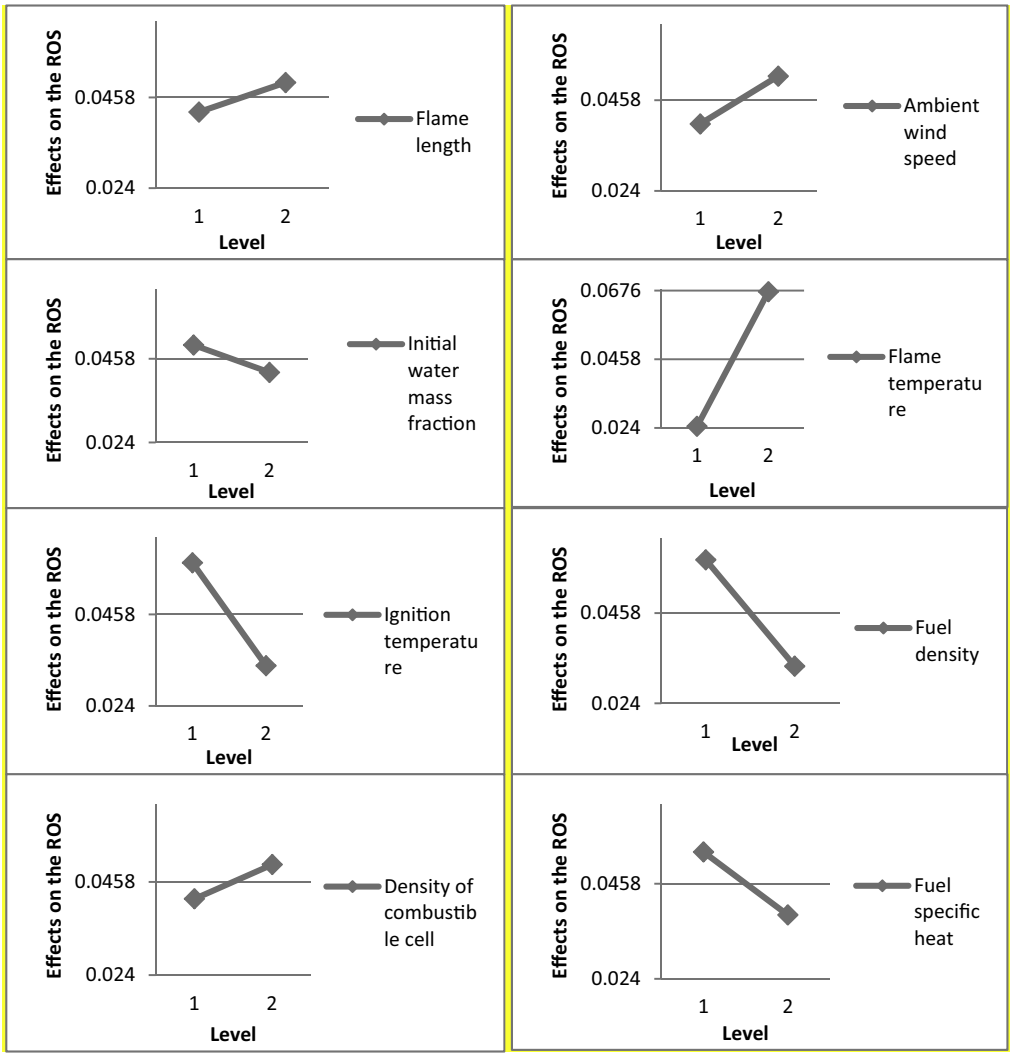

Fig. 6. Curve of influence of parameters on the rate of fire spread (ROS).

temperature has the greatest effect on the rate of fire spread, followed by the ignition temperature and fuel density. The effect of these two parameters is the same, opposite to that of the flame temperature. Third, there is the fuel specific heat and the wind speed. The least influential parameters are the density of combustible fuel, the initial water mass fraction and the flame length.

It is not surprising that the flame temperature significantly affects the rate of fire spread since radiation from the flame appears to be the dominant heat flux contribution, as shown in Fig. 8. This figure shows time evolutions of heat flux contributions to the fuel cell located in the middle of the domain.

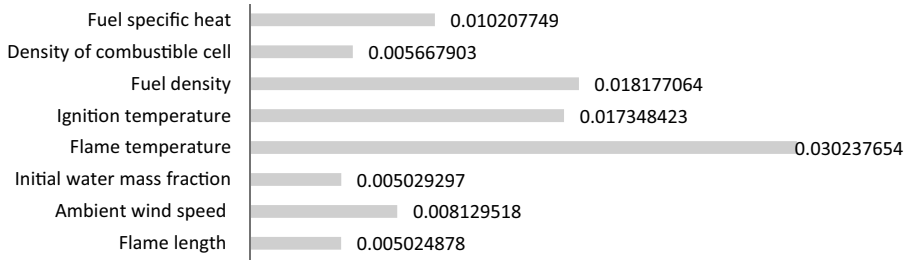

Fig. 7. The standard deviation of the system response.

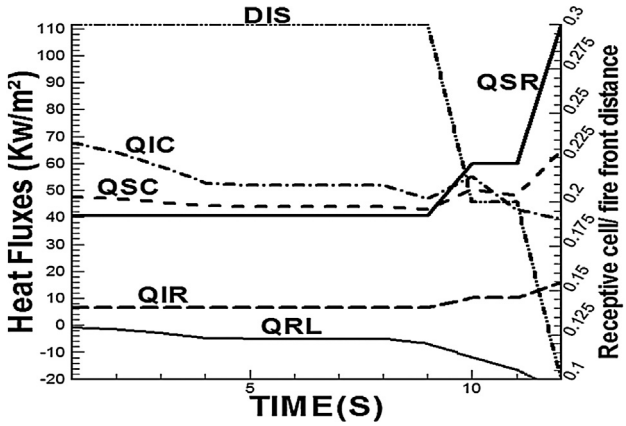

Fig. 8. Time evolutions of the various heat flux contributions to the fuel cell preheating and distance between the receptive cell and the fire front. Here QSR = surface radiation, QIR = internal radiation, QSC = surface convection, QIC = internal convection, QRL = radiative loss, DIS = receptive cell/fire front distance.

5. Conclusion

A fast and simple surface fire model is presented, which combines the features of a network model with those of a semi-physical model of the interaction between the fire and vegetative cells which strongly depends on weather conditions, land topography, and vegetation. Radiation and convection from the flaming zone and embers, and radiative heat loss to the ambient are considered in the preheating process of unburned cells. The predictive capability of the model is partially assessed by comparison with data from laboratory-scale and prescribed burning experiments. Discrepancies between model results and measurements are observed. A better agreement should be obtained by increasing the accuracy with which model parameters are determined. A sensitivity study is performed using a full factorial plan of experiment showing how sensitive the rate of fire spread is to variations in certain model parameters. This could help to identify the parameters we should focus on in the future.

References

[1] B. Porterie, N. Zekri, J.-P. Clerc, J.-C. Loraud, Un réseau de petit monde local à sites pondérés pour les feux de forêts, C. R. Phys. 6 (2005) 151–157.
[2] B. Porterie, N. Zekri, J.-P. Clerc, J.-C. Loraud, Modelling forest fire spread and spotting process with small world networks, Combust. Flame 149 (2007) 63–78.
[3] J.K. Adou, Y. Billaud, D.A. Brou, J.-P. Clerc, J.-L. Consalvi, A. Fuentes, A. Kaiss, F. Nmira, B. Porterie, L. Zekri, Simulating wildfire patterns using a small-world network model, Ecol. Model. 221 (2010) 1463–1471.
[4] G.F. Carrier, F.E. Fendell, M.F. Wolff, Wind-aided firespread across arrays of discrete fuel elements. I: Theory, Combust. Sci. Technol. 75 (1991) 31–51.
[5] M.F. Wolff, G.F. Carrier, F.E. Fendell, Wind-aided firespread across arrays of discrete fuel elements. II: Experiment, Combust. Sci. Technol. 77 (1991) 261–289.
[6] E. Koo, P.J. Pagni, J. Woycheese, S. Stephens, D. Weise, J. Huff, A simple physical model for forest fire spread rate, in: Eighth Symposium on Fire Safety Science, Beijing, 2005.
[7] P.J. Pagni, T.G. Peterson, Flame spread through porous fuel, in: Fourteenth International Symposium on Combustion, The Combustion Institute, (1973), pp. 1099–1107.
[8] W.S.W. Trollope, L.A. Trollope, SAFARI-92 characterization of biomass and fire behavior in the small experimental burns in the Kruger National Park, J. Geophys. Res. 101 (1996) 531–539.
[9] S. Bard, P.J. Pagni, Spatial variation of soot volume fractions in pool fire diffusion flame, in: First Symposium on Fire Safety Science, London, 1985.
[10] G. Hankinson, A method for calculating the configuration factor between a flame and a receiving target for a wide range of flame geometries relevant to large scale fires, in: First Symposium on Fire Safety Science, London, 1985.
[11] F.P. Incropera, D.P. Dewitt, Fundamentals of Heat and Mass Transfer, 4th ed., John Wiley & Sons, 1996.
[12] D.R. Weise, G.S. Biging, A qualitative comparison of fire spread models incorporating wind and slope effects, Forest Sci. 43 (2) (1997) 170–180.
[13] N.P. Cheney, J.S. Gould, W.R. Catchpole, The influence of fuel, weather and fire shape variables on fire spread in grasslands, Int. J. Wildland Fire 3 (1) (1993) 31–44.
[14] D.R. Weise, G.S. Biging, Effects of wind velocity and slope on fire behavior, in: Fourth Symposium on Fire Safety Science, Ottawa, 1994.
[15] N.P. Cheney, J.S. Gould, W.R. Catchpole, Fire growth in grassland fuels, Int. J. Wildland Fire 5 (1995) 237–347.
[16] N.P. Cheney, J.S. Gould, W.R. Catchpole, Prediction of fire spread in grasslands, Int. J. Wildland Fire 8 (1998) 1–13.
[17] M. William, J.J. Charney, M.A. Jenkins, P. Cheney, J. Gould, Numerical simulations of grassland fire behavior from the LANL-FIRETEC and NIST-WFDS models, in: EastFIRE Conference, George Masson University, 2005.